

# Stochastic networks theory to model single-cell genomic count data

Thomas E. Bartlett<sup>1\*</sup>, Swati Chandna<sup>2</sup>, and Sandipan Roy<sup>3</sup>

<sup>1</sup>Department of Statistical Science, University College London, U.K.

<sup>2</sup>Department of Economics, Mathematics and Statistics, Birkbeck University of London, U.K.

<sup>3</sup>Department of Mathematical Sciences, University of Bath, U.K.

\*thomas.bartlett.10@ucl.ac.uk

## Abstract

We propose a novel way of representing and analysing single-cell genomic count data, by modelling the observed data count matrix as a network adjacency matrix. This perspective enables theory from stochastic networks modelling to be applied in a principled way to this type of data, providing new ways to view and analyse these data, and giving first-principles theoretical justification to established, successful methods. We show the success of this approach in the context of three cell-biological contexts, from the epiblast/epithelial/neural lineage. New technology has made it possible to gather genomic data from single cells at unprecedented scale, and this brings with it new challenges to deal with much higher levels of heterogeneity than expected between individual cells. Novel, tailored, computational-statistical methodology is needed to make the most of these new types of data, involving collaboration between mathematical and biomedical scientists.

## 1 Introduction

Network models and methods have become an important subject in modern statistical science, especially in application areas such as cell biology. A network can be represented by an ‘adjacency matrix’ [1], denoted by  $\mathbf{A}$  (Fig.1). In the simplest case, a network consists of nodes of only one type (called a ‘unipartite network’), and these nodes may be connected (or not) by exactly one unweighted edge; in this case,  $\mathbf{A} \in \{0, 1\}^{n \times n}$  (Fig.1a), where  $n$  is the number of nodes in the network. A stochastic network model [2] is a statistical model of a network in which there is a probability of observing an edge between nodes  $i$  and  $j$  defined according to some model, i.e.,  $P(A_{ij} \neq 0) = p_{ij}$ , where the probability  $p_{ij}$  is defined according to a law which may depend on some characteristics of the nodes  $i$  and  $j$ , such as some observed data-vectors  $\mathbf{x}_i$  and  $\mathbf{x}_j$ .

Network models are well established in genomics. However, in genomics network models are typically used to represent gene regulation in a gene regulatory network [3], or related notions such as the gene co-expression network. Gene regulation is the phenomenon in which the protein encoded by one gene activates or represses the expression of another gene. When the expression of one gene regulates the expression of another gene in this way, this individual gene regulation is represented by an edge connecting the repressing and activating genes in the gene regulatory network. However, the focus of the work presented in this paper is not gene regulatory networks. Instead, we use a network model as a novel representation of single-cell genomic count data, and we draw on recent advances in stochastic network modelling to improve clustering and visualisation of the single cells in a genomic data set.

Raw genomic sequencing data (RNA-seq, ATAC-seq, etc) may be represented as a matrix  $\mathbf{X} \in \mathbb{Z}_{\geq 0}^{p \times n}$  of non-negative integer counts. These are counts of genomic sequencing reads, such that each entry  $X_{ij}$  represents the number of observed copies of genomic fragment (e.g., mRNA transcript)  $i \in \{1, \dots, p\}$  in sample (e.g., cell)  $j \in \{1, \dots, n\}$ . Modern single-cell sequencing data use

UMIs (unique molecular identifiers), which avoid double-counting the same transcript (after amplification by PCR, polymerase chain reaction). In these data, the columns of  $\mathbf{X}$  may be modelled as  $n$  independent draws from a multinomial distribution [4]. This contrasts with long-established methods for analysing RNA-seq data which use normalisation methods such as TPM (transcripts per million) and FPKM (fragments per kilobase per million). Normalisation methods such as TPM and FPKM normalise the data by library size (i.e.,  $\sum_{i=1}^p X_{ij}$ ), and this may induce spurious correlations between transcripts [4], as well as making it difficult to write down expressions for the true error distributions of the data after normalisation. In other words, after normalisation, we can't say exactly what the true distribution of the normalised data is, and so rely on heuristics. Instead, we take a unique view of the data that is inspired by stochastic network theory. Our perspective allows data modelling based on a fundamental understanding of the distribution of the data and summaries that follow.

When the genomic data being analysed are the only available observations of some single cells in a study, an important task when analysing these data is to group cells together of similar types for identification or ‘phenotyping’, e.g., by clustering. One of the most successful and reliable methods for clustering single cells in genomic data is the so-called ‘Louvain clustering’ method [5], as implemented in the industry-standard Seurat software package [6]. Louvain clustering works by optimising an estimator called the ‘network modularity’, which is defined in Section 2.2. Another important task when analysing single-cell data is visualisation of the data by projection into two dimensions, e.g., using non-linear methods such as UMAP (uniform manifold approximation and projection) or  $t$ -SNE ( $t$ -distributed stochastic neighbour embedding). The main aim of these projections is that data points which are close together in the original high dimensional space should remain close together in the two dimensional projection, where distance between points is quantified by a carefully chosen metric (e.g. the  $t$ -statistic). The  $p$  features of data matrix  $\mathbf{X} \in \mathbb{R}^{p \times n}$  usually contain much redundancy, and so to aid computational tractability and reduce noise [7], spectral methods may be used to reduce the dimension of the data to  $\mathbf{Y} \in \mathbb{R}^{d \times n}$  where  $d \ll p$ , before using a non-linear method such as  $t$ -SNE or UMAP to generate the two dimensional projection  $\tilde{\mathbf{Y}} \in \mathbb{R}^{2 \times n}$  from  $\mathbf{Y}$ . It is natural to carry out spectral clustering and non-linear projection using the same spectral decomposition  $\mathbf{Y}$  of the data-matrix  $\mathbf{X}$ .

The structure of this papers is as follows. In Section 2, we present our novel first-principles representation of single-cell genomic count data, and our improved method of clustering single cells, that we call ‘GMM-LE’ clustering, and related visualisations. Then in Section 3, we present the results of applying GMM-LE clustering and related visualisation to example data-sets relevant to human cortical development, to human embryonic development, and to breast cancer initiation, showing an improvement over the state-of-the-art methods that are currently available.

## 2 Methods

### 2.1 Model specification

The model specification is based on the observation that a single-cell genomic data-matrix  $\mathbf{X} \in \mathbb{Z}_{\geq 0}^{p \times n}$  has equivalent characteristics to the adjacency matrix  $\mathbf{A}$  that represents a bipartite network with multi-edges (Fig.1b). By ‘multi-edges’ we mean that a pair of nodes may be connected by multiple edges, I.e.,  $A_{ij} \in \mathbb{Z}_{\geq 0}$ . By ‘bipartite’ we mean that the network can have nodes of two different types (represented by blue circles and red squares in Fig.1b), and in our setting we restrict this so that only nodes of different types may be connected by edges. Furthermore, both  $\mathbf{A}$  and  $\mathbf{X}$  tend to be very sparse (i.e., contain a large proportion of zeros: typically less than 10% of the matrix elements are non-zero in both cases). Hence, modelling  $\mathbf{X}$  with  $\mathbf{A}$  provides a mathematical justification for using clustering methodology designed for networks, as described in Section 2.2. We note that this adjacency matrix is  $\mathbf{A} \in \mathbb{Z}_{\geq 0}^{p \times n}$ , and our model is thus specified as  $\mathbf{A} = \mathbf{X}$ .

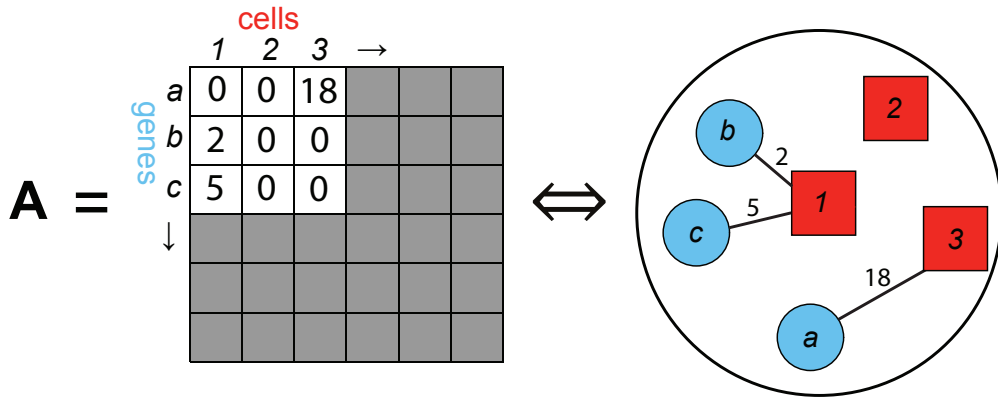
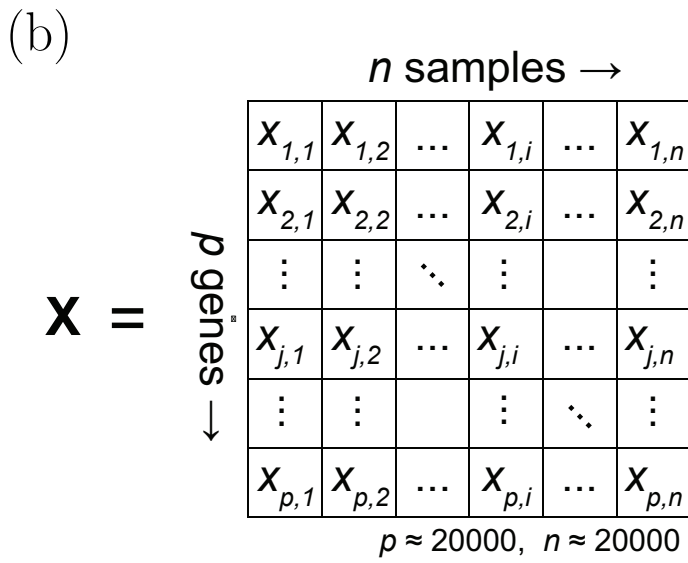
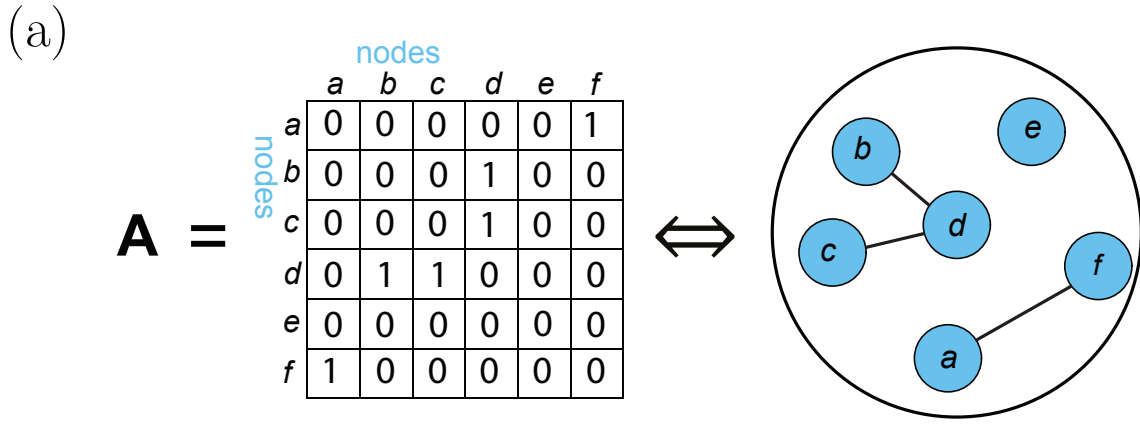


**Figure 1: Network model of count data.** (a) Adjacency matrix  $\mathbf{A} \in \{0, 1\}^{n \times n}$  represents a symmetric unipartite network. (b) Adjacency matrix  $\mathbf{A} \in \mathbb{Z}_{\geq 0}^{p \times n}$  represents an asymmetric bipartite multi-edge network; adjacency matrix  $\mathbf{A}$  (and the equivalent network it represents) models the data matrix  $\mathbf{X}$  of non-negative integer counts.

## 2.2 Single-cell data clustering

Communities in a network are groups of highly interconnected nodes in that network (Fig.2). Assigning network nodes  $i \in \{1, \dots, n\}$  to communities is an equivalent problem to clustering the nodes

[8], and hence when these nodes represent single cells, community detection methodology can be used to cluster single cells. When the data-matrix  $\mathbf{X}$  is high dimensional, as is typical in genomics, this can lead to poor performance of standard clustering methodology such as  $K$ -means. This is because as the dimensionality of the data increases, the euclidean distances between similar and dissimilar points converge, making it difficult to cluster similar points together. As a result, dimension reduction is often used to project the  $n$  data-points represented by  $\mathbf{X}$  into a lower dimensional subspace  $\mathbf{Y} \in \mathbb{R}^{d \times n}$ , before carrying out the clustering in that  $d < p$  dimensional subspace. When the dimension reduction is carried out by spectral methods such as PCA (principal components analysis) or SVD (singular value decomposition), this procedure is called spectral clustering.

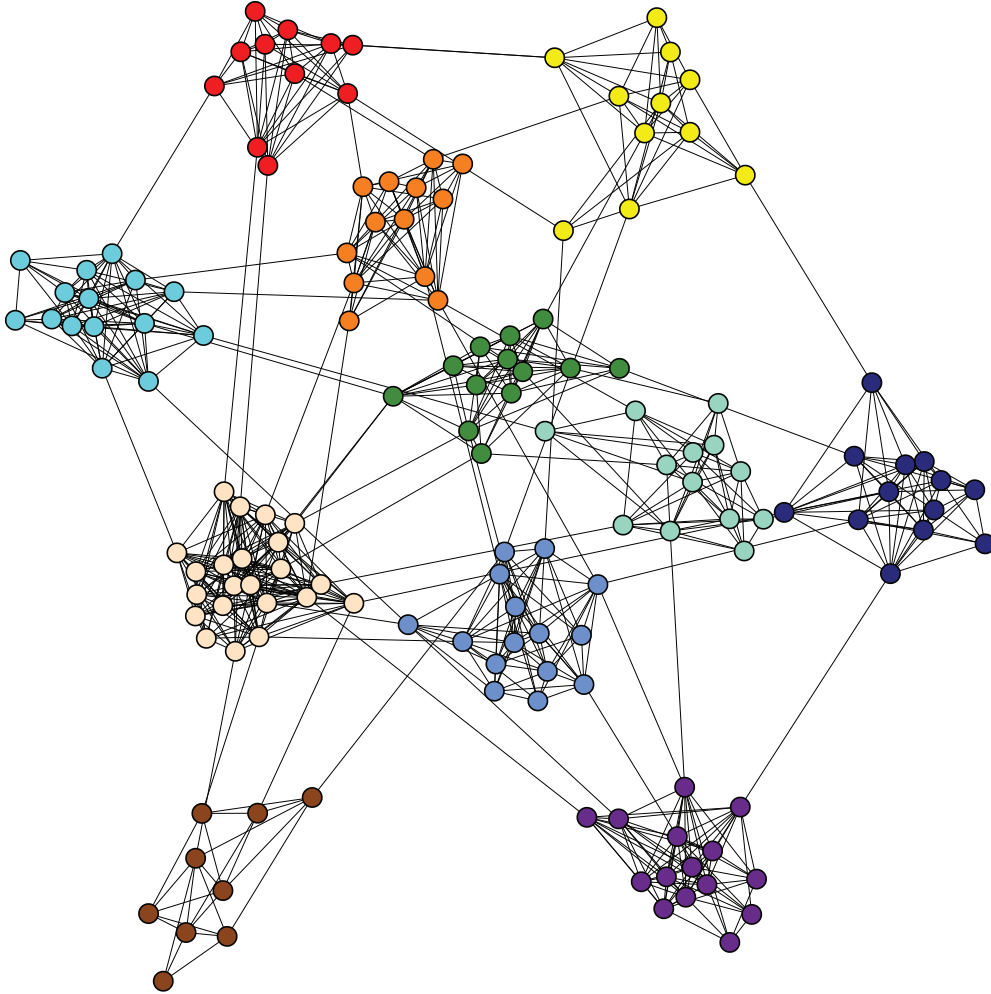


**Figure 2: Communities in a network.** Network nodes in the same community are displayed with the same colour. The density of network edges tends to be much greater within communities, than between communities.

Newman equated spectral clustering of network nodes with maximising an estimator called the network modularity [8], and these concepts are described as follows. We start with a network of  $n$  nodes represented by the adjacency matrix  $\mathbf{A} \in \{0, 1\}^{n \times n}$ , where  $A_{ij} = 1$  and  $A_{ij} = 0$  correspond (respectively) to the presence or absence of an edge in the network between nodes  $i$  and  $j$ . Then, spectral clustering of the nodes proceeds with  $\mathbf{A}$  as the ‘input matrix’ (i.e., the input to the spectral clustering algorithm), or alternatively with its ‘graph-Laplacian’  $\mathcal{L} = \mathbf{D}^{-1/2} \mathbf{A} \mathbf{D}^{-1/2}$  as the ‘input matrix’, where  $\mathbf{D}$  is the diagonal matrix of the vector  $(D_1, D_2, \dots, D_n)^\top$ , with  $D_i = \sum_{j=1}^n A_{ij}$ . Taking either  $\mathbf{A}$  or  $\mathcal{L}$  as the ‘input matrix’, spectral clustering first carries out dimension-reduction to give the matrix  $\mathbf{Y} \in \mathbb{R}^{d \times n}$ , before carrying out  $K$ -means or another type of clustering in this

$d < n$  dimensional subspace. When spectral methods are used to project the graph-Laplacian representation of the  $n$  data-points into a dimensionally-reduced subspace  $\mathbf{Y} \in \mathbb{R}^{d \times n}$ , we refer to this subspace as the ‘Laplacian eigenspace’, or ‘Laplacian spectral embedding’ (LSE). On the other hand, when spectral methods are used to project the adjacency matrix representation of the data-points into a dimensionally-reduced subspace, we refer to this subspace as the ‘adjacency spectral embedding’ (ASE) [9].

The network modularity is defined as an aggregated ‘observed minus expected’ statistic  $Q(\mathbf{C})$ , given cluster labels  $\mathbf{C} = \{c_1, c_2, \dots, c_K\}$ , where  $c_k$  is the set of nodes labelled as cluster  $k \in \{1, \dots, K\}$ :

$$Q(\mathbf{C}) = \frac{1}{D^{++}} \sum_{i=1}^n \sum_{j=1}^n \left( A_{ij} - \frac{D_i D_j}{D^{++}} \right) \cdot \mathbb{I}[\zeta(i) = \zeta(j)],$$

where node degree  $D_i = \sum_{j=1}^n A_{ij}$ , total number of edges  $D^{++} = \sum_{i=1}^n D_i = \sum_{i=1}^n \sum_{j=1}^n A_{ij}$ , and indicator function  $\mathbb{I}[\zeta(i) = \zeta(j)] = 1$  if nodes  $i$  and  $j$  appear together in any set of cluster labels  $c \in \mathbf{C}$ , or  $\mathbb{I}[\zeta(i) = \zeta(j)] = 0$  otherwise, where  $c = \zeta(i)$  means that node  $i$  is assigned to cluster  $c$ . Recent research has shown that clusters in the eigenspace of either the adjacency matrix  $\mathbf{A}$  or its corresponding graph-Laplacian  $\mathcal{L}$  asymptotically follow multivariate Gaussian distributions [10]. Therefore, fitting a Gaussian mixture model (GMM), rather than  $K$ -means clustering, is better specified for the eigenspace of either the matrix  $\mathbf{A} = \mathbf{X}$  or of its graph-Laplacian  $\mathcal{L} = \mathbf{D}^{-1/2} \mathbf{A} \mathbf{D}^{-1/2}$ . Therefore, in the results presented in Section 3, we fit a Gaussian mixture model (GMM) in the Laplacian eigenspace, a procedure we refer to as GMM-LE clustering. We note that inferred clusters obtained using a Gaussian mixture model with diagonal covariance matrices are effectively the same as the clusters obtained from the  $K$ -means algorithm.

### 2.3 Single-cell data visualisation

Single-cell data are often visualised in two dimensions by using non-linear methods such as UMAP or  $t$ -SNE, i.e., projecting the data  $\mathbf{X} \in \mathbb{Z}_{\geq 0}^{p \times n}$  to give  $\tilde{\mathbf{Y}} \in \mathbb{R}^{2 \times n}$ . To aid computational tractability and reduce noise, spectral decomposition is often applied to the data matrix to give  $\mathbf{Y} \in \mathbb{R}^{d \times n}$ ,  $d \ll p$ , before carrying out non-linear projection to  $\tilde{\mathbf{Y}} \in \mathbb{R}^{2 \times n}$  for visualisation [7]. Therefore it is natural to carry out spectral clustering and non-linear projection of the data based on the same spectral decomposition of the data matrix  $\mathbf{X}$ . We suggest that when clustering the data-points in the Laplacian eigenspace, it is most natural to obtain the two-dimensional projection of these  $n$  data-points by applying non-linear dimension reduction to the representation of these data-points in the Laplacian eigenspace, i.e., the eigendecomposition of  $\mathcal{L} = \mathbf{D}^{-1/2} \mathbf{A} \mathbf{D}^{-1/2}$ . In Section 3, we present visualisations of various single-cell genomic data-sets that are based on applying UMAP to the projection of the data points into the Laplacian eigenspace, a procedure that we refer to as UMAP-LE (uniform manifold approximation and projection from the Laplacian eigenspace).

## 3 Results

In this section, we use the methodology described in Section 2, to cluster and visualise single-cell genomic data from three recent studies from different cell-biological contexts:

- *Human cortical development* [11]: data for  $p = 15735$  RNA transcripts in  $n = 31073$  cells, from the V1 area of the visual cortex in the brains of human embryos at gestation weeks 20-22.
- *Human embryonic development* [12]: data for  $p = 20407$  RNA transcripts in  $n = 1258$  cells, from the blastocyst stage of the embryo at 5-7 days post fertilisation.
- *Breast cancer initiation* [13]: data for  $p = 14835$  RNA transcripts in  $n = 17730$  cells, from the epithelial lineage and supporting cells, from human breast tissue from healthy individuals.

Fig.3, Fig.4, and Fig.5 show clustering and visualisation based on the Laplacian eigenspace estimated from respectively, the human cortical development data-set, the human embryonic development data-set, and the breast cancer initiation data-set. UMAP is used to project the  $n$  data-points into two dimensions for visualisation, based on their projection into the estimated Laplacian eigenspace (UMAP-LE). GMM-LE clustering is also carried out by fitting a Gaussian mixture model in the same estimated Laplacian eigenspace. In the plots in these figures, each dot represents one cell (sample). In the cluster plots, the colours indicate the GMM-LE cluster that the cell is assigned to. In the remaining plots, the colours indicate the average log-expression levels of sets of marker genes defined for specific cell-types that are relevant to each data-set. These sets of marker genes have been used previously by us in other studies relating to human neural development [14], human embryonic development [15], and breast cancer initiation [16].

### 3.1 Human cortical development dataset: visualisation and clustering inferences

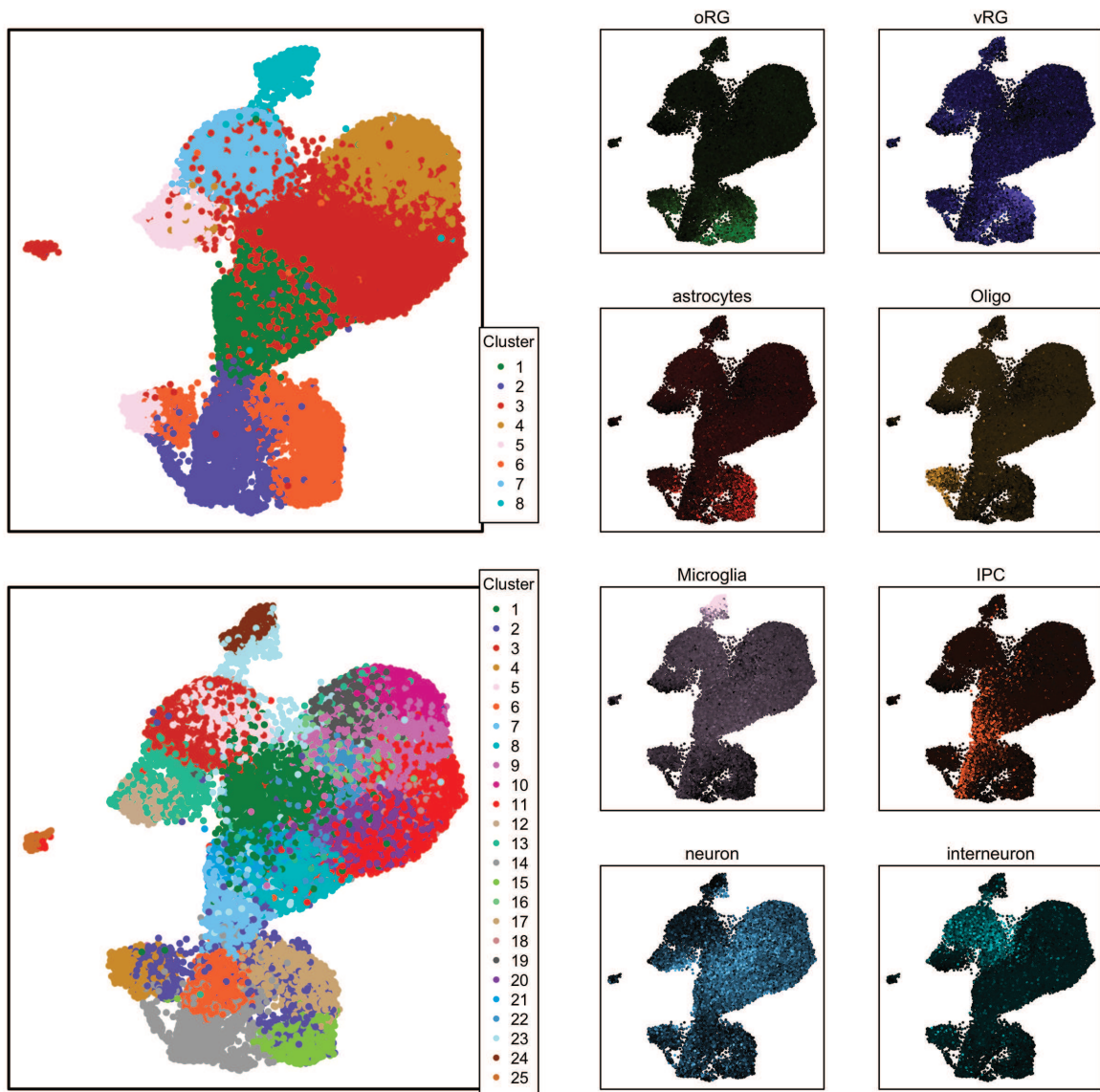


**Figure 3: Projection, clustering, and validation, for the human cortical development data-set.** UMAP projections from the Laplacian eigenspace (UMAP-LE) show GMM-LE clusters and mean expression levels of validating marker genes for cell-types of interest.

The cell-type validation plots shown in Fig.3 illustrate that the UMAP projection of the data-

points in the Laplacian eigenspace (UMAP-LE) make biological sense. The neural stem-cell types oRG (outer radial glia) and vRG (ventricular radial glia) appear in separate yet close locations, and a trajectory can be discerned from these stem-cell types through IPC (intermediate progenitor cells) to neuron and interneurons. The GMM-LE clusters also closely correspond to the greatest colour intensity in the validation plots for specific cell-types. However, the number of clusters  $K$  is an important parameter to set in any clustering procedure. Because the validation for the clustering in the human cortical development data-set was based on marker genes for 8 different neural cell-types, we started with  $K = 8$  clusters for this data-set (Fig.3). However, this did not lead to the neural stem-cell types oRG (outer radial glia) and vRG (ventricular radial glia) being clustered separately, despite their apparent separation in the UMAP projection of the Laplacian eigenspace. Therefore, we tested  $K \in \{5, 10, 15, 20, 25\}$ , finding that  $K \in \{20, 25\}$  provided sufficient granularity to separate the neural stem-cell types oRG and vRG, with little difference in the clustering output between  $K = 20$  and  $K = 25$ . However, at this level of granularity, it becomes clear that the definitions of ‘neuron’ (i.e., excitatory neurons) and ‘interneuron’ (i.e., inhibitory neurons) are too broad for our sets of validation markers, and that finer definitions of neuronal subtypes will be required to identify these (possibly novel) subtypes. We also compared these results from GMM-LE clustering against those obtained from the well-known Louvain clustering algorithm [5] implemented in the industry-standard Seurat software package [6]. The Seurat software with default settings chooses  $K = 22$ , and therefore we used  $K = 22$  to compare results between the GMM-LE and Seurat-Louvain clustering methods. Table 1 shows ratios of the mean log expression of the marker genes for one cell-type to the mean log expression for the markers for all the other cell-types. These are based on cell-type identity assigned to each cluster based on the set of markers with the greatest mean expression level in each cluster. For 6 out of 8 cell-types, GMM-LE clustering performs better; however as noted already, the worse performance for neurons and interneurons is likely to be due to the fact that these definitions are too broad for clustering at this level of granularity, and therefore these general cell-types span several clusters.

Method	oRG	vRG	astrocytes	Oligo	Microglia	IPC	neuron	interneuron
GMM-LE	1.43	1.16	1.29	1.56	1.44	1.56	1.17	1.41
Seurat-Louvain	1.31	1.09	1.25	1.58	1.29	1.29	1.16	1.97

**Table 1: Comparison of GMM-LE clustering and Seurat-Louvain clustering in the human cortical development data-set.** Ratios of the mean log expression of marker genes for the cell-type of interest to the other cell-types are shown.

### 3.2 Human embryonic development dataset: visualisation and clustering inferences

Research on human embryos is highly restricted, due to ethical and regulatory considerations. This constrains sample sizes in generated data-sets, restricting inferences that can be obtained from these samples. If a novel clustering method is able to increase the number of cells obtained from an embryo that can be reliably identified as a specific cell-type of interest in the embryo such as epiblast cells, then it would be potentially very valuable to biological science researchers because it would increase the effective sample size for these precious cells that can be used for further research based on those data. Epiblast cells are precursors to the ectoderm layer, one of three primary germ layers of the embryo; epiblast cells go on to form neural and epithelial cells [17]. Using GMM-LE clustering, we were able to increase the number of cells that can be reliably identified as epiblast from a well-known study of human embryos [12], compared to the latest research in the field [18]. To set the number of clusters  $K$  shown in Fig.4, we increased  $K$  until the epiblast cells formed a distinct cluster as shown by the UMAP projection of the Laplacian eigenspace (UMAP-LE), setting  $K = 8$ . In Fig.4, cluster 5 identifies 68 epiblast cells according to expression of the marker genes NANOG and KLF17, and the absence of expression of GATA3 and SOX17 [19]. These 68 cells include 44 of 45 cells that were previously identified as epiblast, as well as very importantly 24 cells

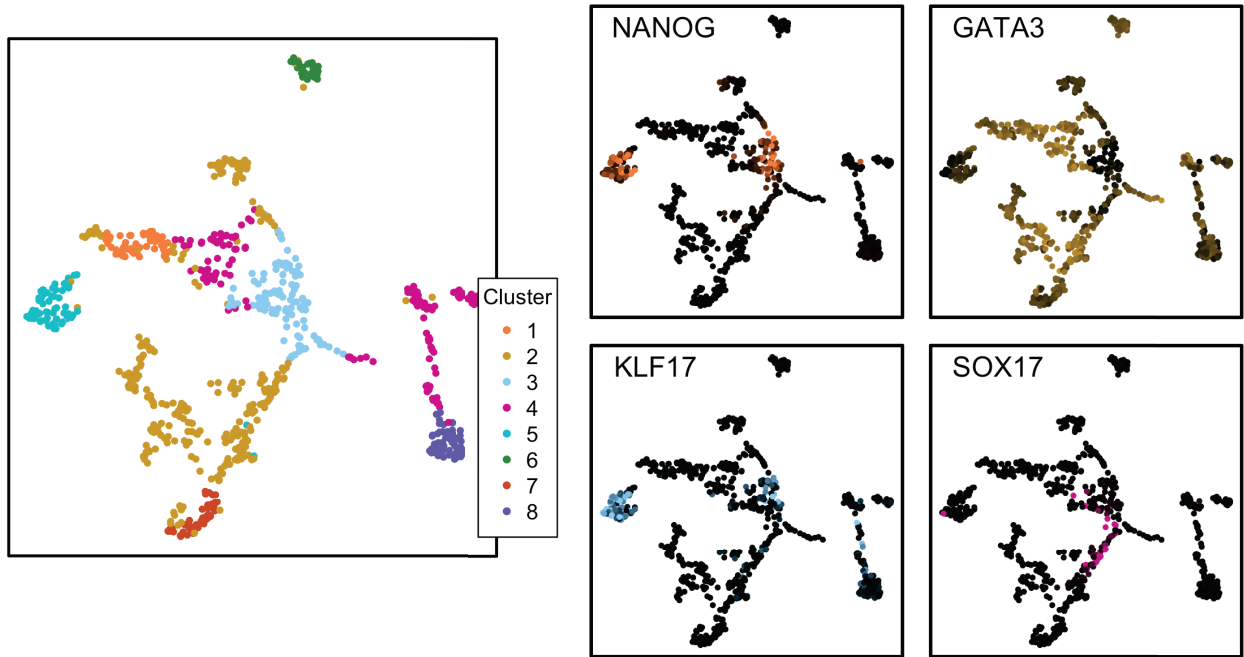


**Figure 4: Projection, clustering, and validation, for the human embryonic development data-set.** UMAP projections from the Laplacian eigenspace (UMAP-LE) show GMM-LE clusters and expression levels of validating marker genes for cell-types of interest.

newly identified as epiblast cells here. The full list of all 68 epiblast cells are given in Appendix B.

### 3.3 Breast cancer initiation dataset: visualisation and clustering inferences

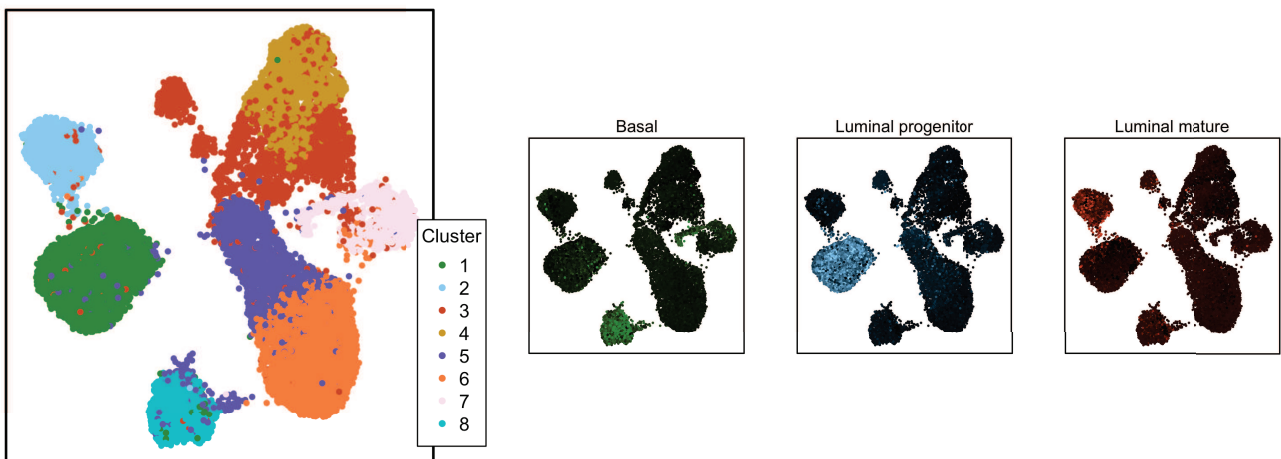


**Figure 5: Projection, clustering, and validation, for the breast cancer initiation data-set.** UMAP projections from the Laplacian eigenspace (UMAP-LE) show GMM-LE clusters and mean expression levels of validating marker genes for cell-types of interest.

The main cell-types of the epithelial lineage in breast tissue are luminal progenitor cells and mature luminal cells (thought to be the cells-of-origin of, respectively, hormone-receptor negative and positive breast cancers) as well as basal cells [20]. As luminal progenitor cells are thought to be the cell-of-origin of highly aggressive triple negative breast cancers (TNBC), it is important to be able to identify these cells as accurately as possible, e.g., for quantifying their numbers in tissue samples from at-risk individuals. Important applications of accurately quantifying luminal



progenitor cells include developing novel biomarkers and surrogate end-points for clinical trials of chemopreventative medicines [21]. We have previously shown that GMM-LE clustering improves identification of luminal progenitor cells in single-cell genomic data compared to Seurat-Louvain clustering [16]. In this study we identify the breast epithelial subtypes basal, luminal progenitor, and mature luminal cells in a different recently published data-set [13], again showing an improvement over Seurat-Louvain clustering (Table 2). The breast epithelial subtypes can be well separated in the UMAP projection of the data-points in the Laplacian eigenspace (UMAP-LE), and they can be separated well by GMM-LE clustering, as illustrated by Fig.5. To carry out GMM-LE clustering here, we again increased the number of clusters  $K$  until the breast epithelial subtypes were well separated, choosing  $K = 8$ .

Method	Basal	Luminal progenitor	Luminal mature
GMM-LE	2.017	1.994	1.561
Seurat-Louvain	1.993	1.978	1.560

**Table 2: Comparison of GMM-LE clustering and Seurat-Louvain clustering in the breast cancer initiation data-set.** Ratios of the mean log expression of marker genes for the cell-type of interest to the other cell-types are shown.

## 4 Discussion

In this paper we have presented a novel first-principles method of modelling single-cell genomic count data, by modelling these data as a network adjacency matrix. This view of single-cell genomic data opens up a wealth of new modelling approaches for this type of data based on stochastic networks theory. It also gives theoretical validation to well-established and highly successful methods for clustering these data based on community detection, such as Louvain clustering [5]. In particular, this view shows the promise of studying the eigenspace of the graph-Laplacian (the ‘Laplacian eigenspace’) to identify and represent known and novel cell-types. Based on this, we have proposed a new method of visualising single-cell genomic data based on the UMAP projection of the representation of the data-points in the Laplacian eigenspace (UMAP-LE), and we have proposed GMM-LE clustering, or ‘Gaussian mixture modelling in the Laplacian eigenspace’. We show that UMAP-LE visualisations correspond to existing biological knowledge, and that GMM-LE clustering outperforms the industry standard clustering method for these data, i.e., the implementation of Louvain clustering in the Seurat software.

There are several outstanding questions still to address in this research. In particular, choosing the number of clusters for a particular data-set is a challenging problem, which we have addressed heuristically for each data-set here. Developing an automatic method for choosing the number of clusters for GMM-LE clustering is a priority. A straightforward approach to this problem is to set the number of clusters as one greater than the dimensionality of the Laplacian eigenspace that is used [22]. We note that the latent dimensionality of the eigenspace of the graph-Laplacian can be estimated using existing theory based on scree plots [23]. Recent findings from stochastic network modelling provides refined methodology to choose the optimum number of clusters to estimate in the Laplacian eigenspace via the Bayesian Information Criterion (BIC) [9]. Building on existing theory for bootstrapping network data with latent structure [24] will enable estimates of uncertainty to be calculated for estimators of the number of latent clusters, as well as quantifying uncertainty on the estimated Laplacian eigenspace. We also note that there are alternative methods for calculating the graph-Laplacian, such as the random-walk Laplacian [25], which will be interesting to investigate in relation to single-cell genomic data. Finally, we have previously proposed a novel method of estimating a latent space in which different cell-types or clusters can be separated well, based on the Mahalanobis distance [16]. It will be interesting to investigate how this relates to the estimate of the Laplacian eigenspace, and refines it for identifying different cell-types from single-cell genomic data..

In summary, our proposed methodological advances in this work provide mathematical technologies that have the potential for large impact in biomedical science. This is achieved by providing theoretical justification for and improvement on existing and widely adopted methodology for identifying important cell-types in single-cell genomic data.

## 5 References

- [1] R. Bose. “Strongly regular graphs, partial geometries and partially balanced designs”. *Pacific Journal of Mathematics* 13.2 (1963), pp. 389–419.
- [2] P. Erdős and A. Rényi. “On the evolution of random graphs”. *Magyar Tud. Akad. Mat. Kutató Int. Közl* 5 (1960), pp. 17–61.
- [3] D. Bray. “Protein molecules as computational elements in living cells”. *Nature* 376.6538 (1995), pp. 307–312.
- [4] F. W. Townes, S. C. Hicks, M. J. Aryee, and R. A. Irizarry. “Feature selection and dimension reduction for single-cell RNA-Seq based on a multinomial model”. *Genome biology* 20.1 (2019), pp. 1–16.
- [5] V. D. Blondel, J.-L. Guillaume, R. Lambiotte, and E. Lefebvre. “Fast unfolding of communities in large networks”. *Journal of statistical mechanics: theory and experiment* 2008.10 (2008), P10008.
- [6] R. Satija et al. “Spatial reconstruction of single-cell gene expression data”. *Nature biotechnology* 33.5 (2015), pp. 495–502.
- [7] A. L. Haber et al. “A single-cell survey of the small intestinal epithelium”. *Nature* 551.7680 (2017), pp. 333–339.
- [8] M. E. Newman. “Modularity and community structure in networks”. *Proceedings of the national academy of sciences* 103.23 (2006), pp. 8577–8582.
- [9] C. E. Priebe et al. “On a two-truths phenomenon in spectral graph clustering”. *Proceedings of the National Academy of Sciences* 116.13 (2019), pp. 5995–6000.
- [10] P. Rubin-Delanchy, J. Cape, M. Tang, C. E. Priebe, et al. “A statistical interpretation of spectral embedding: the generalised random dot product graph”. *Journal of the Royal Statistical Society Series B* 84.4 (2022), pp. 1446–1473.
- [11] A. Bhaduri et al. “An atlas of cortical arealization identifies dynamic molecular signatures”. *Nature* 598.7879 (2021), pp. 200–204.
- [12] S. Petropoulos et al. “Single-cell RNA-seq reveals lineage and X chromosome dynamics in human preimplantation embryos”. *Cell* 165.4 (2016), pp. 1012–1026.
- [13] B. Pal et al. “A single-cell RNA expression atlas of normal, preneoplastic and tumorigenic states in the human breast”. *The EMBO journal* 40.11 (2021), e107333.
- [14] T. E. Bartlett, I. Kosmidis, and R. Silva. “Two-way sparsity for time-varying networks with applications in genomics”. *The Annals of Applied Statistics* 15.2 (2021), pp. 856–879.
- [15] G. Alanis-Lobato et al. “MICA: A multi-omics method to predict gene regulatory networks in early human embryos”. *bioRxiv* (2023), pp. 2023–02.
- [16] T. E. Bartlett, P. Jia, S. Chandna, and S. Roy. “Inference of tissue relative proportions of the breast epithelial cell types luminal progenitor, basal, and luminal mature”. *Scientific reports* 11.1 (2021), pp. 1–10.
- [17] S. Wainwright. *Langman’s Medical Embryology*. 2010.
- [18] G. G. Stirparo et al. “Integrated analysis of single-cell embryo data yields a unified transcriptome signature for the human pre-implantation epiblast”. *Development* 145.3 (2018), dev158501.
- [19] P. Blakeley et al. “Defining the three cell lineages of the human blastocyst by single-cell RNA-seq”. *Development* 142.18 (2015), pp. 3151–3165.
- [20] P. Tharmapalan, M. Mahendralingam, H. K. Berman, and R. Khokha. “Mammary stem cells and progenitors: targeting the roots of breast cancer for prevention”. *The EMBO journal* 38.14 (2019), e100852.

- [21] T. E. Bartlett et al. “Antiprogestins reduce epigenetic field cancerization in breast tissue of young healthy women”. *Genome medicine* 14.1 (2022), pp. 1–18.
- [22] M. A. Riolo and M. Newman. “First-principles multiway spectral partitioning of graphs”. *Journal of Complex Networks* 2.2 (2014), pp. 121–140.
- [23] M. Zhu and A. Ghodsi. “Automatic dimensionality selection from the scree plot via the use of profile likelihood”. *Computational Statistics & Data Analysis* 51.2 (2006), pp. 918–930.
- [24] K. Levin and E. Levina. “Bootstrapping networks with latent space structure”. *arXiv preprint arXiv:1907.10821* (2019).
- [25] A. Modell and P. Rubin-Delanchy. “Spectral clustering under degree heterogeneity: a case for the random walk Laplacian”. *arXiv preprint arXiv:2105.00987* (2021).
- [26] W. E. Johnson, C. Li, and A. Rabinovic. “Adjusting batch effects in microarray expression data using empirical Bayes methods”. *Biostatistics* 8.1 (2007), pp. 118–127.
- [27] D. J. McCarthy, Y. Chen, and G. K. Smyth. “Differential expression analysis of multifactor RNA-Seq experiments with respect to biological variation”. *Nucleic acids research* 40.10 (2012), pp. 4288–4297.

## 6 Appendix A: Data-sets and data pre-processing

The human cortical development data-set was downloaded from the NeMO (Neuroscience Multi-Omic) data archive from URL:

[https://data.nemoarchive.org/biccn/grant/u01\\_devhu/kriegstein/transcriptome/scell/10x\\_v2/human](https://data.nemoarchive.org/biccn/grant/u01_devhu/kriegstein/transcriptome/scell/10x_v2/human)

Data for 33694 RNA transcripts in 44885 cells were downloaded, corresponding to cells from the V1 area of the visual cortex from four embryos at 20–22 gestation weeks. After quality control and filtering, data for 15735 features (RNA transcripts) in 31073 samples (cells) remained, and were carried forward for the subsequent modelling and analysis.

The human embryonic development data-set was downloaded from the ArrayExpress repository under accession number E-MTAB-3929, from URL:

<https://www.ebi.ac.uk/biostudies/arrayexpress/studies/E-MTAB-3929>

Data for 26178 RNA transcripts in 1529 cells were downloaded, corresponding to cells from the blastocyst stage of embryonic development. After quality control and filtering to retain cells from embryos at 5–7 days post-fertilisation, data for 20407 features (RNA transcripts) in 1258 samples (cells) remained, and were carried forward for the subsequent modelling and analysis.

The breast cancer initiation data-set was downloaded from the Gene Expression Omnibus (GEO) repository under accession number GSE161529, from URL:

<https://www.ncbi.nlm.nih.gov/geo/query/acc.cgi?acc=GSE161529>

Data for 33538 RNA transcripts in 26272 cells were downloaded, corresponding to cells from the epithelial lineage and supporting cells. After quality control, data for 14835 features (RNA transcripts) in 17730 samples (cells) remained, and were carried forward for the subsequent modelling and analysis.

For quality control, high quality features (RNA transcripts) and samples (cells) were retained by filtering out any RNA transcripts with non-zero counts in fewer than 50 cells, and by filtering out any cells with non-zero counts for fewer than 750 RNA transcripts, filtering out cells for which the most highly expressed transcript excluding MALAT1 account for at least 10% of the total counts, filtering out cells for which at least 10% of the total counts correspond to transcripts encoding mitochondrial proteins, and filtering out cells for which at least 50% of the total counts correspond to transcripts encoding ribosomal proteins. For the human embryonic data-set, features were instead filtered out if they have non-zero counts in fewer than 10 samples (cells), noting the smaller sample size for this data-set; also for the human embryonic data-set no filtering was carried out based on transcripts encoding mitochondrial proteins because they did not appear in the data-set. For the human cortical development data-set and the breast cancer initiation data-set, batch correction using the COMBAT software [26] was also applied to remove inter-individual differences.

After quality control, the top features were selected for dimension reduction, visualisation, and clustering, according to an estimator of the amount of biological variability compared to technical variability [27] in each feature  $i \in \{1, \dots, p\}$  defined as  $\log V_i / \log m_i$ , where  $V_i$  and  $m_i$  are the empirical variance and mean for feature  $i$ , respectively. The top 2000 features were retained in this way for the human cortical development data-set and the breast cancer initiation data-set, and the top 5000 features were retained for the embryonic development data-set. We note that this procedure in practice approximates a standard technique for obtaining the features with the greatest biological variability in which a line of best fit is found for a plot of  $\log V_i$  against  $\log m_i$ , and the features that are furthest above this line are then selected. This practice is based on the assumption that the data for feature  $i$  will follow a Poisson distribution when only technical variation is present meaning that  $V_i \approx m_i$ , and will be overdispersed when biological variation is present meaning that  $V_i \approx m_i + \phi_i m_i^2$ , where  $\phi_i > 0$  is an overdispersion parameter for feature  $i$  [27]. The Laplacian eigenspace is then estimated as the space defined by the eigendecomposition of the graph-Laplacian, according to the eigenvectors that correspond to the eigenvalues that explain at least 1% of the total variance of the graph-Laplacian representation of the data-points.

## 7 Appendix B: Human embryo epiblast cells identified in this study.

E6.10.1046	E6.17.1588	E6.9.1024	E7.17.1348
E6.10.1048	E6.17.1611	E7.10.760	E7.17.1353
E6.10.1049	E6.17.1612	E7.10.761	E7.6.262
E6.10.1050	E6.17.1617	E7.10.762	E7.6.264
E6.10.1051	E6.22.1852	E7.10.764	E7.8.311
E6.10.1052	E6.22.1866	E7.10.766	E7.8.312
E6.10.1055	E6.8.791	E7.10.768	E7.8.317
E6.10.1056	E6.8.792	E7.12.858	E7.8.318
E6.10.1057	E6.8.794	E7.12.861	E7.8.329
E6.10.1058	E6.8.801	E7.12.869	E7.8.333
E6.12.1274	E6.8.802	E7.12.871	E7.8.343
E6.12.1289	E6.8.813	E7.14.895	E7.9.547
E6.13.1378	E6.8.815	E7.17.1334	E7.9.554
E6.13.1381	E6.8.816	E7.17.1335	E7.9.556
E6.13.1389	E6.8.820	E7.17.1342	E7.9.562
E6.16.1501	E6.8.821	E7.17.1346	E7.9.569
E6.17.1586	E6.9.1022	E7.17.1347	E7.9.571

**Table 3: The 68 epiblast cells identified in Section 3.2.** The listed cell IDs correspond to the IDs given in the original study that generated these data [12].